

The Convex Matching Distance in Multiparameter Persistence

Francesco Conti Patrizio Frosini Ulderico Fugacci Eloy Mosig García
 Nicola Quercioli Sara Scaramuccia Francesca Tombari

Abstract

We introduce the convex matching distance, a novel metric for comparing functions with values in the real plane. This metric measures the maximal bottleneck distance between the persistence diagrams associated with the convex combinations of the two function components. Similarly to the traditional matching distance, the convex matching distance aggregates the information provided by two real-valued components. However, whereas the matching distance depends on two parameters, the convex matching distance depends on only one, offering improved computational efficiency. We further show that the convex matching distance can be more discriminative than the traditional matching distance in certain cases, although the two metrics are generally not comparable. Moreover, we prove that the convex matching distance is stable and characterize the coefficients of the convex combination at which it is attained. Finally, we demonstrate that this new aggregation framework benefits from the computational advantages provided by the Pareto grid, a collection of curves in the plane whose points lie in the image of the Pareto critical set associated with functions assuming values on the real plane. Experimental validation on MNIST digits, synthetic shapes, and chaotic attractors suggests that the convex matching distance provides a reliable and efficient alternative to the matching distance, at a significantly lower computational cost.

Keywords

Biparameter persistent homology, Matching distance, Pareto grid.

1 Introduction

In recent years, research on multiparameter persistent homology has grown substantially, driven by the need to apply Topological Data Analysis (TDA) techniques to data represented by multifiltrations, as occurs, for example, when analysing or comparing data described by vector-valued functions [33, 7, 17, 14, 16, 15, 18, 23, 19, 22, 39, 3, 35]. However, a fully developed theoretical framework enabling efficient applications of TDA in this setting is still lacking. A widely adopted comparison method in multiparameter persistence is based on the *matching distance* [26, 8, 20, 37, 4, 9]. This pseudo-metric is introduced by observing that, given a continuous function $\varphi : X \rightarrow \mathbb{R}^n$ representing the data of interest, we can consider monoparametric filtrations of the topological space X associated with lines in \mathbb{R}^n having direction given by a vector $\mathbf{a} = (a_1, \dots, a_n)$ such that $\sum_{i=1}^n a_i = 1$ and $a_1, \dots, a_n > 0$. Each such line, parametrised as $\mathbf{b} + u\mathbf{a}$ with $\mathbf{b} = (b_1, \dots, b_n)$ and $\sum_{i=1}^n b_i = 0$, induces a filtration $\{X_u^{(\mathbf{a}, \mathbf{b})}\}_{u \in \mathbb{R}}$ of X defined by the subsets $X_u^{(\mathbf{a}, \mathbf{b})}$ consisting of all points in X whose image under φ has coordinates less than or equal to those of $\mathbf{b} + u\mathbf{a}$. From an analytical viewpoint, this construction is equivalent to considering, for each function $\varphi = (\varphi_1, \dots, \varphi_n) : X \rightarrow \mathbb{R}^n$, the sublevel sets of the real-valued function

$$\varphi_{\mathbf{a}, \mathbf{b}}^*(p) := \min_{1 \leq i \leq n} \{a_i\} \max_{1 \leq i \leq n} \left\{ \frac{\varphi_i(p) - b_i}{a_i} \right\}. \quad (1)$$

With this premise, the matching distance in degree k between two continuous functions $\varphi, \psi : X \rightarrow \mathbb{R}^n$ is defined by setting

$$d_{\text{match}, k}(\varphi, \psi) := \sup_{\mathbf{a}, \mathbf{b}} d_B(\text{Dgm}_k(\varphi_{\mathbf{a}, \mathbf{b}}^*), \text{Dgm}_k(\psi_{\mathbf{a}, \mathbf{b}}^*)),$$

where d_B is the bottleneck distance and Dgm_k is the operator that computes the persistence diagrams in degree k .

In recent years, the extended Pareto Grid has been introduced to compute points in the persistence diagram of $\varphi_{\mathbf{a}, \mathbf{b}}^*$, and to characterise at which (\mathbf{a}, \mathbf{b}) the matching distance is attained [21, 27, 32].

While the study of the matching distance is geometrically interesting and theoretically rich it involves $2(n-1)$ independent parameters and depends non-smoothly on the function φ , leading to computational challenges and monodromy [21]. We address this issue by considering the operator that maps a function

$$\varphi = (\varphi_1, \dots, \varphi_n): X \rightarrow \mathbb{R}^n$$

to a family of real-valued functions $\varphi^{\mathbf{t}}$ defined as follows: for each $\mathbf{t} = (t_1, \dots, t_n) \in \mathbb{R}^n$ satisfying $\sum_{i=1}^n t_i = 1$ and $t_i \geq 0$ for all i , we set

$$\varphi^{\mathbf{t}} := \sum_{i=1}^n t_i \varphi_i.$$

The conditions on \mathbf{t} imply $t_n = 1 - \sum_{i=1}^{n-1} t_i$; hence, the family $\{\varphi^{\mathbf{t}}\}_{\mathbf{t} \in \mathbb{R}^n}$ depends on $n-1$ parameters, substantially reducing the complexity of the approach based on the parameters \mathbf{a} and \mathbf{b} . Moreover, our operator $F_{\mathbf{t}}(\varphi) = \varphi^{\mathbf{t}}$ depends smoothly on the parameters \mathbf{t} and the function φ , in contrast with the operator in (1).

Furthermore, the operator $F_{\mathbf{t}}$ gives rise to a new pseudo-metric between filtering functions, called the *convex matching distance*, defined as

$$\mathbf{cmd}_k(\varphi, \psi) := \max_{\substack{t_1, \dots, t_n \geq 0 \\ t_1 + \dots + t_n = 1}} d_B(\text{Dgm}_k(\varphi^{\mathbf{t}}), \text{Dgm}_k(\psi^{\mathbf{t}})).$$

Although this pseudo-metric is not always more discriminative than the classical matching distance (as shown by Examples 1 and 2), its dependence on $n-1$ parameters, together with the fact that it is defined via a smooth procedure, provides significant computational advantages from an applied perspective.

The theoretical framework from which the convex matching distance derives is that of *group equivariant non-expansive operators (GENEOs)*, which were introduced ten years ago to restrict the invariance of persistence diagrams in Topological Data Analysis [31]. In particular, the convex matching distance originates from the paper [5], where it was proved that selecting an arbitrary family of GENEOs leads to the construction of new stable matching distances (Proposition 9 and Theorem 10; see also [29]). In the present paper, we focus on the family of operators $F_{\mathbf{t}}(\varphi) = \varphi^{\mathbf{t}}$, which yields the convex matching distance, owing to the interesting computational properties of this metric. Interestingly, infinitely many other examples of parametric families of GENEOs can be defined. For instance, restricting ourselves to monoparametric families, we may consider the following operators:

$$\hat{F}_t(\varphi) := (1-t) \max(\varphi_1, \varphi_2) + t \min(\varphi_1, \varphi_2), \quad t \in [0, 1],$$

and

$$\tilde{F}_t(\varphi) := \left(\frac{1}{2}|\varphi_1|^t + \frac{1}{2}|\varphi_2|^t\right)^{\frac{1}{t}}, \quad t \geq 1.$$

Each of these operators could be used to define new pseudo-metrics in TDA. We emphasize that the theory of GENEOs also has interesting applications beyond classical Topological Data Analysis (cf., e.g., [5, 41, 2, 10, 12, 25, 28, 11, 13, 38, 1]).

For alternative approaches to this idea of a unifying theory to generate distances in persistence, we refer to [6] where projected distances between multiparameter persistence modules are introduced in the context of sheaf theoretic persistence. The convex matching distance can also be framed in this context.

The approach described in this paper is related to, but distinct from, the *persistent homology transform (PHT)* [45]. The PHT is a topological transform that takes as input a subset of a Euclidean space and associates to every unit vector the collection of persistence diagrams of the height functions on that subset in the direction given by the vector. A distance between two subsets is then defined by integrating over the sphere the distances between the respective persistence diagrams. The convex matching distance, instead, is obtained as a maximum over the unit vectors of non-negative slope, thus, over a smaller set. Considering only vectors of positive slope is a crucial aspect of our techniques because, together with some regularity assumptions, it enables the use of a convenient differential geometry tool, called the *Pareto grid*. Another key difference between the two approaches lies in their scope. While the PHT is designed to recover the geometry of the object X , our method, based on convex combinations of a vector-valued function, focuses on making inferences about the function whose domain is X .

In this paper, we study the convex matching distance in the case $n = 2$. We prove that the convex matching distance is stable with respect to the uniform norm $\|\varphi - \psi\|_{\infty}$ (Proposition 2) and establish a *Position Theorem* (Theorem 2), analogous to the one already known for the matching distance [21, 32]. This theorem allows one to recover, from the Pareto grid of φ , the coordinates of the points in the

persistence diagram of $\varphi^t := (1-t)\varphi_1 + t\varphi_2$, for every $t \in [0, 1]$. Finally, in Theorem 3, we show that the convex matching distance coincides with the maximal bottleneck distance between the persistence diagrams of the functions φ^t and ψ^t for t belonging to a suitable set of special values, thus paving the way for an efficient method to compute the convex matching distance.

We validate the practical effectiveness of the convex matching distance through experiments on three benchmark datasets: MNIST digit classification, synthetic 3D shapes under varying noise levels, and chaotic dynamical attractors. Our results highlight that the convex matching distance achieves comparable classification performance to the matching distance computed on a fine 11×11 parameter grid, while requiring only 11 persistence diagram computations instead of 121. Moreover, we observe that the convex matching distance can outperform coarser approximations of the matching distance, confirming that the convex parametrization captures the essential discriminative information of the bifiltration. These findings establish the convex matching distance as a computationally efficient and theoretically grounded alternative to existing multiparameter persistence metrics.

2 Preliminaries

In this section, we recall the bottleneck distance in monoparameter persistence and the matching distance in biparameter persistence. To do that, some preliminary notions about persistence theory is needed, and certain hypothesis need to be assumed. However, as this is fairly standard, we will not delve into details, and refer the reader to [32, Section 2 and Appendix A] for a compact treatment of preliminaries. The following is a complete list of symbols used in this article ¹:

- X is a compact topological space;
- $\Delta := \{(u, u) \mid u \in \mathbb{R}\}$, $\Delta^+ := \{(u, v) \mid u, v \in \mathbb{R}, u < v\}$, $\bar{\Delta}^* := \Delta^+ \cup \{(u, \infty) \mid u \in \mathbb{R}\} \cup \{\Delta\}$;
- $\text{Dgm}_k(\varphi)$ is the k -th persistence diagram of the continuous function $\varphi: X \rightarrow \mathbb{R}$, and it is a multiset in $\bar{\Delta}^*$, where each of its points has a multiplicity, and, in particular, Δ is a point in $\text{Dgm}_k(\varphi)$ with infinite multiplicity;
- the following function $d: \bar{\Delta}^* \times \bar{\Delta}^* \rightarrow [0, \infty]$ is an extended metric

$$d(p, q) := \begin{cases} C(u, u', v, v') & \text{if } p = (u, v), q = (u', v') \in \Delta^+, \\ |u - u'| & \text{if } p = (u, \infty), q = (u', \infty), \\ \frac{v-u}{2} & \text{if } p = (u, v) \in \Delta^+, = \Delta, \\ \frac{v'-u'}{2} & \text{if } p = \Delta, q = (u', v') \in \Delta^+, \\ 0 & \text{if } p = q = \Delta, \\ \infty & \text{otherwise,} \end{cases}$$

where $C(u, u', v, v') := \min\{\max\{|u - u'|, |v - v'|\}, \max\{\frac{v-u}{2}, \frac{v'-u'}{2}\}\}$;

- if $\varphi = (\varphi_1, \varphi_2): X \rightarrow \mathbb{R}^2$ continuous function, $\varphi_{\mathbf{a}, \mathbf{b}}^* := \min\{a, 1 - a\} \max\{\frac{\varphi_1 - b}{a}, \frac{\varphi_2 + b}{1 - a}\}$, with $\mathbf{a} := (a, 1 - a)$, $\mathbf{b} := (b, -b)$, and $a \in]0, 1[$, $b \in \mathbb{R}$.

Let $\varphi, \psi: X \rightarrow \mathbb{R}$ be continuous functions. The k -bottleneck distance [24] is a metric between persistence diagrams defined by

$$d_{B,k}(\varphi, \psi) := d_B(\text{Dgm}_k(\varphi), \text{Dgm}_k(\psi)) = \max_{\sigma} \max_{p \in \text{Dgm}_k(\varphi)} d(p, \sigma(p)),$$

where σ ranges over the multiset bijections between $\text{Dgm}_k(\varphi)$ and $\text{Dgm}_k(\psi)$.

Let $\varphi, \psi: X \rightarrow \mathbb{R}^2$ be continuous functions. The k -th matching distance [20] is a metric between the persistence Betti number functions (rank invariants) defined by

$$d_{\text{match},k}(\varphi, \psi) := \sup_{\mathbf{a}, \mathbf{b}} d_{B,k}(\varphi_{\mathbf{a}, \mathbf{b}}^*, \psi_{\mathbf{a}, \mathbf{b}}^*).$$

Remark 1. Because of the definition of d , the k -bottleneck distance between persistence diagrams $\text{Dgm}_k(\varphi)$ and $\text{Dgm}_k(\psi)$ is of the form $c|w_0 - w_1|$, where $c \in \{\frac{1}{2}, 1\}$, and w_0, w_1 are coordinates of the points of $\text{Dgm}_k(\varphi) \sqcup \text{Dgm}_k(\psi)$.

¹Note that these symbols might differ slightly from those used in [32].

3 Convex matching distance

Let us consider a continuous function $\varphi = (\varphi_1, \varphi_2): X \rightarrow \mathbb{R}^2$. For every $t \in [0, 1]$, we set $\varphi^t := (1-t)\varphi_1 + t\varphi_2$.

Definition 1. Considering $\varphi, \psi: X \rightarrow \mathbb{R}^2$ and an integer k , we define the *convex matching distance* \mathbf{cmd}_k between φ and ψ as

$$\mathbf{cmd}_k(\varphi, \psi) := \max_{t \in [0, 1]} d_{B, k}(\varphi^t, \psi^t) = \max_{t \in [0, 1]} d_B(\text{Dgm}_k(\varphi^t), \text{Dgm}_k(\psi^t)). \quad (2)$$

Remark 2. We now show that (2) is well defined and that the maximum actually exists. If the function $\varphi = (\varphi_1, \varphi_2)$ is fixed, then for any $t_1, t_2 \in [0, 1]$ we have

$$\begin{aligned} \|\varphi^{t_1} - \varphi^{t_2}\|_\infty &= \|(1-t_1)\varphi_1 + t_1\varphi_2 - ((1-t_2)\varphi_1 + t_2\varphi_2)\|_\infty \\ &= \|\varphi_1 - t_1\varphi_1 + t_1\varphi_2 - \varphi_1 + t_2\varphi_1 - t_2\varphi_2\|_\infty \\ &= \|(t_1 - t_2)(\varphi_2 - \varphi_1)\|_\infty \\ &= |t_1 - t_2| \|\varphi_1 - \varphi_2\|_\infty. \end{aligned}$$

It follows that the map $t \mapsto \varphi^t$ is $\|\varphi_1 - \varphi_2\|_\infty$ -Lipschitz (see also [6, Proposition 7.9]). From the stability of the matching distance [20]—which implies $d_{B, k}(\varphi^{t_1}, \varphi^{t_2}) \leq \|\varphi^{t_1} - \varphi^{t_2}\|_\infty$ and $d_{B, k}(\psi^{t_1}, \psi^{t_2}) \leq \|\psi^{t_1} - \psi^{t_2}\|_\infty$ —and by applying the triangle inequality, we get

$$\begin{aligned} \left| d_{B, k}(\varphi^{t_1}, \psi^{t_1}) - d_{B, k}(\varphi^{t_2}, \psi^{t_2}) \right| &\leq d_{B, k}(\varphi^{t_1}, \varphi^{t_2}) + d_{B, k}(\psi^{t_1}, \psi^{t_2}) \\ &\leq \|\varphi^{t_1} - \varphi^{t_2}\|_\infty + \|\psi^{t_1} - \psi^{t_2}\|_\infty \\ &\leq |t_1 - t_2| \|\varphi_1 - \varphi_2\|_\infty + |t_1 - t_2| \|\psi_1 - \psi_2\|_\infty. \end{aligned}$$

It follows that the map $t \mapsto d_{B, k}(\varphi^t, \psi^t)$ is continuous on $[0, 1]$, as claimed.

We also observe that the map $\varphi \mapsto \varphi^t$ is 1-Lipschitz for every $t \in [0, 1]$, since

$$\begin{aligned} \|\varphi^t - \psi^t\|_\infty &= \|(1-t)\varphi_1 + t\varphi_2 - ((1-t)\psi_1 + t\psi_2)\|_\infty \\ &= \|(1-t)(\varphi_1 - \psi_1) + t(\varphi_2 - \psi_2)\|_\infty \\ &\leq (1-t)\|\varphi_1 - \psi_1\|_\infty + t\|\varphi_2 - \psi_2\|_\infty \\ &\leq (1-t)\|\varphi - \psi\|_\infty + t\|\varphi - \psi\|_\infty \\ &= \|\varphi - \psi\|_\infty. \end{aligned}$$

Remark 3. If φ is k -times differentiable, with k possibly infinite, then so it is the function φ^t for each $t \in [0, 1]$, due to being defined as the composition of $\varphi = (\varphi_1, \varphi_2)$ with the smooth function $(s_1, s_2) \mapsto (1-t)s_1 + ts_2$. This is a key difference between the convex matching distance and the classical matching distance, for the operator sending φ to $\varphi_{a, b}^*$ preserves continuity only.

Moreover, the function $t \mapsto \varphi^t$ defined on the interval $[0, 1]$ is smooth (i.e., infinitely differentiable) on $[0, 1]$ (where for the endpoints we mean that the function has continuous left-sided or right-sided derivatives of all required orders). The claim has been already proven for the order 0 in Remark 2. For the other orders, it is enough to notice that, independently from the chosen t , the first derivative of the considered function is $-\varphi_1 + \varphi_2$ while, for higher orders, the derivative is the null function.

Remark 4. We call \mathbf{cmd}_k the *convex matching distance* because it is based on the convex combination of the components of φ and ψ . This idea generalises to the case of functions with values in \mathbb{R}^n : given the function $\varphi = (\varphi_1, \dots, \varphi_n)$, we consider the map assigning to each vector $(t_1, \dots, t_n) \in \mathbb{R}^n$ with $t_i \geq 0$ and $\sum_{i=1}^n t_i = 1$ the function $\varphi^t := \sum_{i=1}^n t_i \varphi_i$.

Proposition 1. \mathbf{cmd}_k is a pseudo-metric.

Proof. It can be easily seen that \mathbf{cmd}_k is a non-negative function, for which the symmetry property and the fact that, for any φ , $\mathbf{cmd}_k(\varphi, \varphi) = 0$ are directly inherited from the bottleneck distance. Thus, to complete the proof, it remains to show that the triangle inequality holds. Since $d_{B, k}$ is a pseudo-metric,

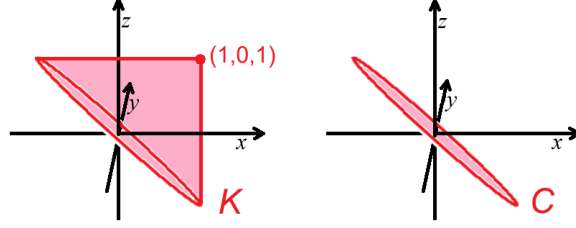


Figure 1: The sets K and C cited in the Examples 1, 2.

for any φ, ψ and ξ we have that

$$\begin{aligned}
\mathbf{cmd}_k(\varphi, \psi) &= \max_{t \in [0,1]} d_{B,k}(\varphi^t, \psi^t) \\
&\leq \max_{t \in [0,1]} (d_{B,k}(\varphi^t, \xi^t) + d_{B,k}(\xi^t, \psi^t)) \\
&\leq \max_{t \in [0,1]} d_{B,k}(\varphi^t, \xi^t) + \max_{t \in [0,1]} d_{B,k}(\xi^t, \psi^t) \\
&= \mathbf{cmd}_k(\varphi, \xi) + \mathbf{cmd}_k(\xi, \psi).
\end{aligned}$$

□

Remark 5. We claim that in general \mathbf{cmd}_k is not a metric. Since there exist two real-valued functions f, g such that $f \neq g$ and $d_B(\text{Dgm}_k(f), \text{Dgm}_k(g)) = 0$, we can consider $\varphi = (f, f)$ and $\psi = (g, g)$. Thus, $\varphi^t = f$ and $\psi^t = g$ for any t . Then we obtain that $\mathbf{cmd}_k(\varphi, \psi) = d_B(\text{Dgm}_k(f), \text{Dgm}_k(g)) = 0$, but $\varphi \neq \psi$.

Proposition 2 (Stability of \mathbf{cmd}_k). *For any k , $\mathbf{cmd}_k(\varphi, \psi) \leq \|\varphi - \psi\|_\infty$.*

Proof. For any $t \in [0, 1]$, by the stability of the bottleneck distance [24] and Remark 2,

$$d_B(\text{Dgm}_k(\varphi^t), \text{Dgm}_k(\psi^t)) \leq \|\varphi^t - \psi^t\|_\infty \leq \|\varphi - \psi\|_\infty.$$

□

4 Comparison with the matching distance

In this section, we compare the newly introduced convex matching distance with the classical matching distance [20].

In Example 1, we exhibit two functions for which the convex matching distance is strictly greater than the classical matching distance, thereby showing that, at least in some cases, the new distance is more discriminative in distinguishing data.

Vice versa, Example 2 provides functions for which the convex matching distance is strictly smaller than the classical matching distance.

Example 1. Let us consider the circumference S in \mathbb{R}^3 of radius $\sqrt{2}$ and center $(0, 0, 0)$, whose points belong to the plane of equation $x + z = 0$. Then, let us consider the circle C bounded by S and the conical set K obtained by taking the union of the segments joining the point $(1, 0, 1)$ to each point of S (see Figure 1). We set $\varphi(x, y, z) := (x, z)$ for $(x, y, z) \in K$ and $\psi(x, y, z) := (x, z)$ for $(x, y, z) \in C$. Given that K and C are homeomorphic to the closed hemisphere $\Sigma := \{(x, y, z) \in \mathbb{R}^3 : x^2 + y^2 + z^2 = 1, x + z \geq 0\}$, we can find two homeomorphisms $\mathbf{h}_K : \Sigma \rightarrow K$, $\mathbf{h}_C : \Sigma \rightarrow C$. Therefore, we can consider the continuous functions $\hat{\varphi} : \Sigma \rightarrow \mathbb{R}^2$, $\hat{\varphi} := \varphi \circ \mathbf{h}_K$, $\hat{\psi} : \Sigma \rightarrow \mathbb{R}^2$, $\hat{\psi} := \psi \circ \mathbf{h}_C$. Let us now compute the following persistence diagrams in degree 1:

$$\text{Dgm}_1(\hat{\varphi}_{a,b}^*) = \text{Dgm}_1(\varphi_{a,b}^*) = \{\Delta\} = \text{Dgm}_1(\psi_{a,b}^*) = \text{Dgm}_1(\hat{\psi}_{a,b}^*) \text{ for any } a, b;$$

$$\text{Dgm}_1(\hat{\varphi}^{\frac{1}{2}}) = \text{Dgm}_1(\varphi^{\frac{1}{2}}) = \{\Delta, (0, 1)\} \text{ and } \text{Dgm}_1(\hat{\psi}^{\frac{1}{2}}) = \text{Dgm}_1(\psi^{\frac{1}{2}}) = \{\Delta\}.$$

Therefore, $d_{\text{match},1}(\hat{\varphi}, \hat{\psi}) = 0$ and $d_B(\hat{\varphi}^{\frac{1}{2}}, \hat{\psi}^{\frac{1}{2}}) = \frac{1}{2}$. Hence $\mathbf{cmd}_1(\hat{\varphi}, \hat{\psi}) \geq \frac{1}{2} > 0 = d_{\text{match},1}(\hat{\varphi}, \hat{\psi})$.

However, the convex matching distance is not always greater than the classical matching distance, as shown by the following example.

Example 2. If we consider degree 0 instead of degree 1, the functions given in Example 1 show a case in which the convex matching distance is strictly smaller than the classical matching distance. In fact, it is easy to verify that

$$\text{Dgm}_0\left(\hat{\varphi}_{\left(\frac{1}{2}, \frac{1}{2}\right), (0,0)}^*\right) = \text{Dgm}_0\left(\varphi_{\left(\frac{1}{2}, \frac{1}{2}\right), (0,0)}^*\right) = \{\Delta, (0, 1), (0, \infty)\};$$

$$\text{Dgm}_0\left(\hat{\psi}_{\left(\frac{1}{2}, \frac{1}{2}\right), (0,0)}^*\right) = \text{Dgm}_0\left(\psi_{\left(\frac{1}{2}, \frac{1}{2}\right), (0,0)}^*\right) = \{\Delta, (0, \infty)\};$$

$$\text{Dgm}_0\left(\hat{\varphi}^t\right) = \text{Dgm}_0\left(\varphi^t\right) = \{\Delta, (1 - 2t, \infty)\} = \text{Dgm}_0\left(\psi^t\right) = \text{Dgm}_0\left(\hat{\psi}^t\right) \text{ for any } t \in [0, 1].$$

Therefore, $d_{\text{match},0}(\hat{\varphi}, \hat{\psi}) \geq \frac{1}{2}$ and $d_B(\text{Dgm}_0(\varphi^t), \text{Dgm}_0(\psi^t)) = 0$ for any $t \in [0, 1]$. Hence, $\mathbf{cmd}_0(\hat{\varphi}, \hat{\psi}) = 0 < \frac{1}{2} \leq d_{\text{match},0}(\hat{\varphi}, \hat{\psi})$.

Remark 6. The above examples can be suitably modified to satisfy more restrictive conditions on the smoothness of the involved functions or on their domains, taken to be manifolds. This shows that their existence is not due to a lack of regularity properties but rather follows from the very definition of the two distances. By identifying the boundaries of two disjoint copies of K and C , respectively, the above examples can be adapted, thus obtaining two smooth functions $\tilde{\varphi}, \tilde{\psi}: \mathbb{S}^2 \rightarrow \mathbb{R}^2$ such that:

- $d_{\text{match},1}(\tilde{\varphi}, \tilde{\psi}) = 0 < \frac{1}{2} \leq \mathbf{cmd}_1(\tilde{\varphi}, \tilde{\psi})$;
- $\mathbf{cmd}_0(\tilde{\varphi}, \tilde{\psi}) = 0 < \frac{1}{2} \leq d_{\text{match},0}(\tilde{\varphi}, \tilde{\psi})$.

5 Pareto grid and Position Theorem

Let M be a closed (i.e., compact and without boundary) smooth Riemannian manifold of dimension $r \geq 2$ and $\varphi = (\varphi_1, \varphi_2): M \rightarrow \mathbb{R}^2$ a smooth function.

- Definition 2.**
1. The *Jacobi set*, $\mathbb{J}(\varphi)$, is the set of all points $x \in M$ at which the gradients of φ_1 and φ_2 are linearly dependent, namely $x \in \mathbb{J}(\varphi)$ if and only if there exists $(\lambda_1, \lambda_2) \neq (0, 0)$ such that $\lambda_1 \nabla \varphi_1(x) + \lambda_2 \nabla \varphi_2(x) = 0$.
 2. The *Pareto critical set* of φ , $\mathbb{J}_P(\varphi)$, is the set of all points $x \in \mathbb{J}(\varphi)$ such that there exists $(\lambda_1, \lambda_2) \neq (0, 0)$ with $\lambda_1, \lambda_2 \geq 0$ such that $\lambda_1 \nabla \varphi_1(x) + \lambda_2 \nabla \varphi_2(x) = 0$. The elements of $\mathbb{J}_P(\varphi)$ are called *Pareto critical points*. Note that $\mathbb{J}_P(\varphi)$ contains both the critical points of φ_1 and those of φ_2 .

Unless otherwise specified, throughout the rest of the article the smooth functions considered will satisfy the following conditions.

Assumption 1.

1. No point x exists in M at which both $\nabla \varphi_1(x)$ and $\nabla \varphi_2(x)$ vanish.
2. $\mathbb{J}(\varphi)$ is a 1-dimensional manifold smoothly embedded in M , consisting of finitely many components, each diffeomorphic to a circle.
3. $\mathbb{J}_P(\varphi)$ is a 1-dimensional closed submanifold of $\mathbb{J}(\varphi)$ with boundary.
4. The connected components of $\mathbb{J}_P(\varphi) \setminus \mathbb{J}_C(\varphi)$ are finite in number, each being diffeomorphic to an interval, where $\mathbb{J}_C(\varphi)$ is the set of cusp points of φ , i.e., the set of points of $\mathbb{J}(\varphi)$ at which the restriction of φ to $\mathbb{J}(\varphi)$ fails to be an immersion. In other words, $\mathbb{J}_C(\varphi)$ is the subset of $\mathbb{J}(\varphi)$ where both $\nabla \varphi_1$ and $\nabla \varphi_2$ are orthogonal to $\mathbb{J}(\varphi)$. With respect to any parameterisation of each component, one of φ_1 and φ_2 is strictly increasing and the other is strictly decreasing. Each component may meet critical points of φ_1 or φ_2 only at its endpoints.

We call the closures of the images of the connected components of $\mathbb{J}_P(\varphi) \setminus \mathbb{J}_C(\varphi)$ (proper) *contours* [21], and denote by $\text{Ctr}(\varphi)$ the set of contours of φ . Given two smooth functions $\varphi, \psi: M \rightarrow \mathbb{R}^2$, we set $\text{Ctr}(\varphi, \psi) := \text{Ctr}(\varphi) \cup \text{Ctr}(\psi)$. It is important to observe that Assumption 1 is generic within the class of smooth functions from M to \mathbb{R}^2 [47].

In our setting, we make one further technical assumption.

Assumption 2.

1. The set $\mathbb{J}_C(\varphi)$ of cusp points is empty.
2. Each contour $\alpha \in \text{Ctr}(\varphi)$ is a smooth regular curve in $\mathcal{C}^\infty([0, 1]; \mathbb{R}^2)$.

Definition 3. The *Pareto grid* of φ is the subset of \mathbb{R}^2 defined as the image $\varphi(\mathbb{J}_P(\varphi))$.

Figure 2 shows the Pareto grid of the projection of a 2-sphere in \mathbb{R}^2 .

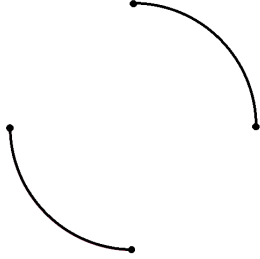


Figure 2: The Pareto grid of the function $\varphi : \mathbb{S}^2 \rightarrow \mathbb{R}^2$ defined by setting $\varphi(x, y, z) := (x, z)$.

Before presenting the main result of this section, we recall the following well-established theorem, which provides a useful relation between the persistence diagram of a smooth function and its critical values. This statement is a technical but standard fact in the literature, and we include it here without proof (cf., e.g., Theorem 3.1 in [42], and [30]).

Theorem 1. *Let M be a closed smooth manifold and $\varphi : M \rightarrow \mathbb{R}$ a smooth function. If w is a finite coordinate of a point $p \in \text{Dgm}_k(\varphi) \setminus \{\Delta\}$, then w is a critical value for φ .*

We are now ready to state the main result of this section. Relying on Theorem 1, it provides a geometric characterisation of the points in the persistence diagram of φ^t in terms of the contours associated with φ . Next theorem is analogous to [21, Theorem 2]. In what follows, the symbol \cdot denotes the dot product.

Theorem 2 (Position Theorem for φ^t). *Let $t \in [0, 1]$ and let w be a finite coordinate of a point in $\text{Dgm}_k(\varphi^t) \setminus \{\Delta\}$. Then there exist a contour denoted as $\alpha = (\alpha_1, \alpha_2) : [0, 1] \rightarrow \mathbb{R}^2$ and a $\bar{\tau} \in [0, 1]$ such that:*

1. $\alpha(\bar{\tau}) \cdot (1 - t, t) = w$;
2. $\frac{d\alpha}{d\tau}(\bar{\tau}) \cdot (1 - t, t) = 0$.

Proof. By Theorem 1 we know that w must be a critical value for φ^t . Therefore, there exists a point $\bar{x} \in M$ such that $w = \varphi^t(\bar{x})$ and $\nabla \varphi^t(\bar{x}) = \mathbf{0}$, where $\mathbf{0}$ denotes the null vector. Hence, $(1 - t)\nabla \varphi_1(\bar{x}) + t\nabla \varphi_2(\bar{x}) = \mathbf{0}$. This means that \bar{x} is a Pareto critical point of φ . Therefore, there exist a contour $\alpha = (\alpha_1, \alpha_2) : [0, 1] \rightarrow \mathbb{R}^2$ and a $\bar{\tau} \in [0, 1]$ such that $\varphi(\bar{x}) = \alpha(\bar{\tau})$, and

$$w = \varphi^t(\bar{x}) = (1 - t)\varphi_1(\bar{x}) + t\varphi_2(\bar{x}) = \varphi(\bar{x}) \cdot (1 - t, t) = \alpha(\bar{\tau}) \cdot (1 - t, t).$$

Consider a smooth regular curve $\gamma : [0, 1] \rightarrow M$ such that $\alpha(\tau) = \varphi \circ \gamma(\tau)$ and $\gamma(\bar{\tau}) = \bar{x}$, which implies that $\alpha(\bar{\tau}) = (\alpha_1(\bar{\tau}), \alpha_2(\bar{\tau})) = (\varphi_1(\gamma(\bar{\tau})), \varphi_2(\gamma(\bar{\tau}))) = (\varphi_1(\bar{x}), \varphi_2(\bar{x}))$. By Assumption 2, $\mathbb{J}_C(\varphi)$ is empty,

hence $\frac{d}{d\tau}(\varphi \circ \gamma(\tau))$ does not vanish for any $\tau \in [0, 1]$. Therefore, we have that

$$\begin{aligned}
0 &= \mathbf{0} \cdot \frac{d\gamma}{d\tau}(\bar{\tau}) \\
&= \nabla \varphi^t(\bar{p}) \cdot \frac{d\gamma}{d\tau}(\bar{\tau}) \\
&= ((1-t)\nabla \varphi_1(\bar{x}) + t\nabla \varphi_2(\bar{x})) \cdot \frac{d\gamma}{d\tau}(\bar{\tau}) \\
&= (1-t)\nabla \varphi_1(\bar{x}) \cdot \frac{d\gamma}{d\tau}(\bar{\tau}) + t\nabla \varphi_2(\bar{x}) \cdot \frac{d\gamma}{d\tau}(\bar{\tau}) \\
&= (1-t)\frac{d\varphi_1 \circ \gamma}{d\tau}(\bar{\tau}) + t\frac{d\varphi_2 \circ \gamma}{d\tau}(\bar{\tau}) \\
&= (1-t)\frac{d\alpha_1}{d\tau}(\bar{\tau}) + t\frac{d\alpha_2}{d\tau}(\bar{\tau}) \\
&= \frac{d\alpha}{d\tau}(\bar{\tau}) \cdot (1-t, t).
\end{aligned} \tag{3}$$

□

It may be useful here to observe how the Position Theorem 2 can be used to find the finite coordinates of the points in $\text{Dgm}_k(\varphi^t) \setminus \{\Delta\}$. The idea is to consider the family of parallel lines having the direction of the vector $(1-t, t)$ and to look for the points where these lines intersect the contours associated with the function $\varphi: M \rightarrow \mathbb{R}^2$ orthogonally. For each such point P , one computes the scalar product $P \cdot (1-t, t)$. As P varies, one thus obtains all the finite coordinates of the points in $\text{Dgm}_k(\varphi^t) \setminus \{\Delta\}$.

6 Special values

For the following definitions we need to introduce the notion of signed radius:

Definition 4. Let α be a regular smooth curve in \mathbb{R}^2 and let $P \in \alpha$. If the curvature of α at P is non-zero, let (x, y) and ρ denote the centre and radius of the osculating circle to α at P , and define the *signed radius* of α at P as $\ell = \text{sign}((P - (x, y)) \cdot (1, 0))\rho$.

Definition 5. The *special set* of (φ, ψ) , denoted by $\text{Sp}(\varphi, \psi)$, consists of the values $t \in [0, 1]$ such that at least one of the following hold:

1. There exists a line r with direction $(1-t, t)$ intersecting orthogonally a contour $\alpha \in \text{Ctr}(\varphi, \psi)$ at one of its endpoints.
2. There exist lines r_1, r_2, r_3, r_4 with direction $(1-t, t)$ and contours $\alpha_1, \alpha_2, \alpha_3, \alpha_4 \in \text{Ctr}(\varphi, \psi)$ such that r_i intersects α_i orthogonally at P_i , for each $i \in \{1, 2, 3, 4\}$, with $\{P_1, P_2\} \neq \{P_3, P_4\}$, and $(P_1 - P_2) \cdot (1-t, t) = c((P_3 - P_4) \cdot (1-t, t))$, for $c \in \{\frac{1}{2}, 1\}$.
3. There exist lines r_1, r_2 with direction $(1-t, t)$ and contours $\alpha_1, \alpha_2 \in \text{Ctr}(\varphi, \psi)$ such that r_i intersects the interior of α_i orthogonally at P_i , for i in $\{1, 2\}$, with $P_1 \neq P_2$ and one of the following conditions holds:
 - α_1 has null curvature at P_1 ,
 - α_2 has null curvature at P_2 ,
 - ℓ_1 and ℓ_2 are defined and $\ell_1 = \ell_2$,
 - ℓ_1 and ℓ_2 are defined, with $\ell_1 \neq \ell_2$, and

$$t = \frac{\zeta}{1 + \zeta} \text{ with } \zeta := \tan \left(\frac{1}{2} \arcsin \left(1 - \left(\frac{(y_1 - y_2) - (x_1 - x_2)}{(\ell_1 - \ell_2)} \right)^2 \right) \right),$$

where ℓ_i is the signed radius and (x_i, y_i) is the center of the osculating circle of α_i at P_i , for i in $\{1, 2\}$.

Remark 7. Note that $t = 0$ and $t = 1$ are always special values for each φ, ψ . For example, to see that $t = 0$ is special, let x in M be a point at which φ_1 attains its maximum. Then $\varphi(x)$ is the endpoint of some contour $\alpha \in \text{Ctr}(\varphi)$. In particular, let $\gamma: [0, 1] \rightarrow M$ be such that $\alpha(\tau) = \varphi \circ \gamma(\tau)$ and suppose that $\gamma(0) = x$. Therefore,

$$0 = \nabla \varphi_1(x) \cdot \frac{d\gamma}{d\tau}(0) = \frac{d(\varphi_1 \circ \gamma)}{d\tau}(0) = \frac{d\alpha_1}{d\tau}(0) = \frac{d\alpha}{d\tau}(0) \cdot (1, 0).$$

Hence $(1, 0)$ is orthogonal to α at an endpoint. One shows in an analogous way that $t = 1$ is also a special value.

Remark 8. The intuition behind Definition 5.2 is the following: if $t \in [0, 1]$ satisfies Definition 5.2, then t is a value at which the optimal matching between $\text{Dgm}(\varphi^t)$ and $\text{Dgm}(\psi^t)$ may change abruptly. In particular, if σ is such an optimal matching and $p_1, p_2, p_3, p_4 \in \text{Dgm}(\varphi^t) \cup \text{Dgm}(\psi^t)$ are such that cost $\sigma = w_1 - w_2 = c(w_3 - w_4)$, where w_i is a finite coordinate of p_i , $i = 1, \dots, 4$, then, in a neighbourhood of t , the optimal matching could be either the one matching p_1 to p_2 or the one matching p_3 to p_4 , but not the other. A similar motivation led to the definition of special set in [27], relatively to the classical matching distance.

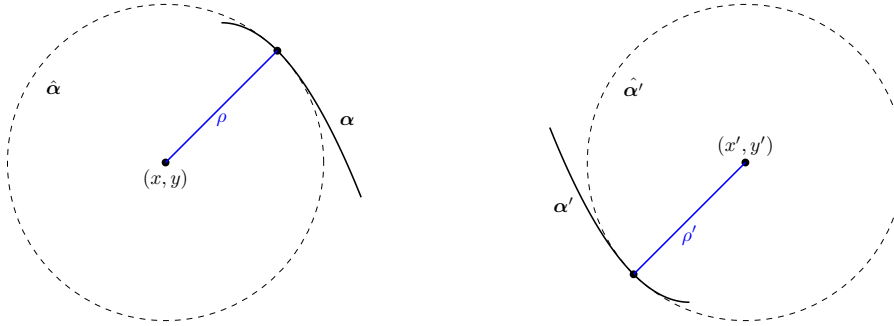


Figure 3: Osculating circles $\hat{\alpha}$ and $\hat{\alpha}'$ of centres $(x, y), (x', y')$ and radii ρ, ρ' to a negative and positive parabola denoted by α and α' , respectively, at a non-critical point. The signed radius ℓ from Definition 4 is positive on the leftmost case and negative on the rightmost one.

Remark 9. We note that the radius ℓ^i appearing in Definition 5.3 has positive sign whenever P_i is above and to the right of the centre of the osculating circle, and negative when it is below and on the left. These are the only cases possible due to Assumption 1.4, which are illustrated in Figure 3.

The next result characterises the values of t at which the convex matching distance is attained. These values always exist by Remark 2. We observe that when the convex matching distance is zero, every $t \in [0, 1]$ realises it.

Theorem 3. *If $\text{cmd}_k(\varphi, \psi) > 0$ and it is realised at \bar{t} , that is,*

$$\text{cmd}_k(\varphi, \psi) = d_{B,k}(\varphi^{\bar{t}}, \psi^{\bar{t}}),$$

then $\bar{t} \in \text{Sp}(\varphi, \psi)$.

Proof. By contradiction, suppose $\bar{t} \notin \text{Sp}(\varphi, \psi)$ and $\text{cmd}_k(\varphi, \psi) = d_{B,k}(\varphi^{\bar{t}}, \psi^{\bar{t}})$.

By Remark 1 there exist coordinates $w_0, w_1 \in \mathbb{R}$ of points in $\text{Dgm}_k(\varphi^{\bar{t}}) \cup \text{Dgm}_k(\psi^{\bar{t}})$ and a constant $c \in \{\frac{1}{2}, 1\}$ such that $\text{cmd}_k(\varphi, \psi) = c|w_0 - w_1| > 0$. Moreover, by Theorem 2, there exist two contours $\alpha, \beta \in \text{Ctr}(\varphi, \psi)$ such that, for some τ_α and τ_β in $[0, 1]$:

$$\begin{aligned} \alpha(\tau_\alpha) \cdot (1 - \bar{t}, \bar{t}) &= w_0, \\ \beta(\tau_\beta) \cdot (1 - \bar{t}, \bar{t}) &= w_1, \end{aligned}$$

where with a slight abuse of notation we denote with $\alpha(\tau), \beta(\tau')$ some smooth parametrisations of α and β such that $(1 - \bar{t}, \bar{t})$ is orthogonal to α and β at $\alpha(\tau_\alpha)$ and $\beta(\tau_\beta)$, respectively. By Definition 5.2 no two distinct pairs of coordinates can realise $d_{B,k}(\varphi^{\bar{t}}, \psi^{\bar{t}})$, hence $\{w_0, w_1\}$ is unique. Moreover,

note that τ_α and τ_β cannot be in $\{0, 1\}$, since 0 and 1 are special values (see Remark 7), it is enough to consider the interior of the contours α and β .

Now, we locally reparametrise the interior of the contours α and β in neighborhoods of $\alpha(\tau_\alpha)$ and $\beta(\tau_\beta)$, respectively. Let $\theta(t) := \arctan\left(\frac{t}{1-t}\right) \in]0, \frac{\pi}{2}[$ for $t \in]0, 1[$ and let $\bar{\theta} := \theta(\bar{t})$. Consider the osculating circles $\hat{\alpha}$ and $\hat{\beta}$ at $\alpha(\tau_\alpha)$ and $\beta(\tau_\beta)$, which may be parametrised as $\hat{\alpha}(\theta) := (x_\alpha, y_\alpha) + \ell_\alpha(\cos \theta, \sin \theta)$ and $\hat{\beta}(\theta) := (x_\beta, y_\beta) + \ell_\beta(\cos \theta, \sin \theta)$, where ℓ_α, ℓ_β and $(x_\alpha, y_\alpha), (x_\beta, y_\beta)$ denote the signed radii – in the sense of Definition 4 – and centres of the osculating circles, and the parameter θ varies in $[0, 2\pi[$. Note that, $\hat{\alpha}(\bar{\theta}) = \alpha(\tau_\alpha)$. Moreover, by Definition 5.3 and Assumption 2, we have $|\ell_\alpha|, |\ell_\beta| \in]0, \infty[$. Consider the line $r(\theta) := \{(x_\alpha, y_\alpha) + s(\cos \theta, \sin \theta) \mid s \in \mathbb{R}\}$, and let $\alpha(\theta)$ be the local and smooth parametrisation of α given by the intersection $\alpha \cap r(\theta)$ in a neighbourhood of $\bar{\theta}$. The existence of this parametrisation is by the transversality between α and $r(\theta)$ provided by Assumption 1.

By reparametrising β in a neighborhood of $\beta(\tau_\beta)$ in the same fashion, we obtain $\beta(\bar{\theta}) = \beta(\tau_\beta)$. Thus, we can consider the difference $w_0(\theta) - w_1(\theta) = \alpha(\theta) \cdot (1-t, t) - \beta(\theta) \cdot (1-t, t)$. To finish the proof we will show that $\dot{w}_0(\bar{\theta}) - \dot{w}_1(\bar{\theta}) \neq 0$, where we denote with the upper dot the derivative with respect to θ .

By definition of θ and osculating circles, we have $\alpha(\bar{\theta}) = \hat{\alpha}(\bar{\theta})$, $\beta(\bar{\theta}) = \hat{\beta}(\bar{\theta})$, $\dot{\alpha}(\bar{\theta}) = \dot{\hat{\alpha}}(\bar{\theta})$ and $\dot{\beta}(\bar{\theta}) = \dot{\hat{\beta}}(\bar{\theta})$. Noting that $(1-t, t) = \left(\frac{\cos \theta}{\cos \theta + \sin \theta}, \frac{\sin \theta}{\cos \theta + \sin \theta}\right)$, we can explicitly compute the derivative $\dot{w}_0(\theta)$ in a neighborhood of $\bar{\theta}$:

$$\begin{aligned} \dot{w}_0(\theta) &= \frac{\partial}{\partial \theta} \left[\alpha(\theta) \cdot \left(\frac{\cos \theta}{\cos \theta + \sin \theta}, \frac{\sin \theta}{\cos \theta + \sin \theta} \right) \right] \\ &= \dot{\alpha}(\theta) \cdot \left(\frac{\cos \theta}{\cos \theta + \sin \theta}, \frac{\sin \theta}{\cos \theta + \sin \theta} \right) + \alpha(\theta) \cdot \frac{(-1, 1)}{(\cos \theta + \sin \theta)^2}. \end{aligned} \quad (4)$$

The denominators in the previous expression do not vanish since $\theta \in]0, \frac{\pi}{2}[$. As $\dot{\alpha}(\bar{\theta}) = \dot{\hat{\alpha}}(\bar{\theta})$, we can rewrite (4) using the parametrisation of the osculating circle $\hat{\alpha}$:

$$\begin{aligned} \dot{w}_0(\bar{\theta}) &= \left[\ell_\alpha(-\sin \theta, \cos \theta) \cdot \left(\frac{\cos \theta}{\cos \theta + \sin \theta}, \frac{\sin \theta}{\cos \theta + \sin \theta} \right) \right. \\ &\quad \left. + ((x_\alpha, y_\alpha) + \ell_\alpha(\cos \theta, \sin \theta)) \cdot \frac{(-1, 1)}{(\cos \theta + \sin \theta)^2} \right]_{\theta=\bar{\theta}} \\ &= \left[\frac{y_\alpha - x_\alpha + \ell_\alpha(\sin \theta - \cos \theta)}{(\cos \theta + \sin \theta)^2} \right]_{\theta=\bar{\theta}}. \end{aligned} \quad (5)$$

By using the osculating circle $\hat{\beta}$ we can replicate the same reasoning to compute $\dot{w}_1(\bar{\theta})$. Subtracting both formulas we obtain:

$$\frac{d}{d\theta} [w_0(\theta) - w_1(\theta)]_{\theta=\bar{\theta}} = 0 \quad \text{if and only if} \quad \cos \bar{\theta} - \sin \bar{\theta} = \frac{(y_\alpha - y_\beta) - (x_\alpha - x_\beta)}{\ell_\alpha - \ell_\beta}, \quad (6)$$

where the radii ℓ_α, ℓ_β have positive or negative sign according to Definition 4.

Note that the denominator on the right-hand side of (6) does not vanish by Definition 5.3. Recall the trigonometric formula $(\cos \theta - \sin \theta)^2 = 1 - \sin 2\theta$, which applied to (6) yields

$$\bar{\theta} = \frac{1}{2} \arcsin \left(1 - \left(\frac{(y_\alpha - y_\beta) - (x_\alpha - x_\beta)}{\ell_\alpha - \ell_\beta} \right)^2 \right).$$

Lastly, applying back the change of variables $\tan \theta = \frac{t}{1-t}$ to the left-hand side of the last equation with $t = \bar{t}$ yields exactly the condition in Definition 5.3, implying $\bar{t} \in \text{Sp}(\varphi, \psi)$. This generates the desired contradiction. \square

Remark 10. In the proof of Theorem 3, we use the fact that the parametrisation of α defined by the intersection $\alpha \cap r(\theta)$ is smooth in a neighborhood of $\alpha(\tau_\alpha)$. The fact that $\alpha(\theta)$ is a well-defined and smooth curve follows from the assumption that all lines passing through the point (x_α, y_α) intersect the contour α transversally.

7 Experiments

Throughout the section, every function $\varphi = (\varphi_1, \varphi_2): X \rightarrow \mathbb{R}^2$ takes values in $[0, 1]^2$. This prevents scale-dependent artifacts in both the convex combinations and the bottleneck distance computations. Moreover, each point cloud will lie in the unit cube. We remind that $\mathbf{a} = (a, 1 - a)$ and $\mathbf{b} = (b, -b)$.

The aim of this section is to evaluate the convex matching distance against the classical matching distance. In practice, both distances are approximated by evaluating the maximum over finite grids. Specifically, we evaluate three scenarios:

- **CMD:** approximation of \mathbf{cmd}_k by restricting to a uniform grid of 11 values $t \in \{0, 0.1, \dots, 1\}$ in the convex combination $(1 - t)\varphi_1 + t\varphi_2$;
- **MD 121:** approximation of $d_{\text{match},k}$ by restricting to a fine 11×11 grid with a ranging from 0.05 to 0.95 and $b \in \{0, 0.1, \dots, 1\}$ in the parameter space for $\varphi_{\mathbf{a},\mathbf{b}}^*, \psi_{\mathbf{a},\mathbf{b}}^*$;
- **MD 10:** approximation of $d_{\text{match},k}$ by restricting to a coarser 2×5 grid with $a \in \{0.25, 0.75\}$ and $b \in \{0, 0.25, 0.5, 0.75, 1\}$.

The goal is to show that CMD provides a reliable alternative for MD 121 (which is approximately 11 times slower), while outperforming MD 10, whose computational cost is comparable to CMD. We conduct three experiments: (i) a direct evaluation of distance quality on MNIST digits (Section 7.1), (ii) a classification task on synthetic shapes (Section 7.2) and (iii) a classification task on chaotic attractors (Section 7.3). We conclude with a dedicated timing analysis (Section 7.4), showing that the empirical computational cost aligns with the expected theoretical speed-up of CMD over the classical matching distance.

All classification experiments use k -nearest neighbors ($k = 3$) with bottleneck distance (tolerance $\varepsilon = 0.01$). Classification is performed using a most-confident selection strategy across H_0 and H_1 , and performance is evaluated via 10-fold cross-validation. Code and results are available at <https://doi.org/10.5281/zenodo.18644292>. Persistent homology computations were carried out using the GUDHI library [40].

7.1 Distance quality on MNIST

The aim of this section is to quantify CMD, MD 121 and MD 10 on MNIST, and assess whether the discriminating power of CMD is comparable to that of MD121, which in turn is higher than that of MD10. To keep the computational cost limited, we selected 100 samples for each of the 10 classes, yielding $\binom{1000}{2} = 499,500$ pairs. Let X denote the 28×28 pixel grid. We define the functions $\varphi_1(x) = I(x)/255$, where $I(x) \in [0, 255]$ is the pixel intensity, and φ_2 as the radial distance from the image center, restricted to active pixels ($I(x) > 50$) and set to 0 otherwise. The function φ_2 is normalised to take values in $[0, 1]$. For persistence computation, we construct a cubical complex on the 28×28 pixel grid, using the superlevel set filtration induced either by φ^t (for CMD) or $\varphi_{\mathbf{a},\mathbf{b}}^*$ (for MD 121 and MD 10).

Figure 4 displays scatterplots comparing the three distances. Each point corresponds to an image pair, with coordinates given by the two distances being compared: for instance, in panel (a), the x -coordinate is CMD and the y -coordinate is MD 121, both computed in homological dimension 0. Points near the diagonal (red dashed line) indicate image pairs where both distances yield similar values, while points far from the diagonal indicate that one distance dominates over the other. As shown in Figure 4 (a, b), CMD and MD 121 are nearly identical in both homological dimensions. In contrast, the comparison between CMD and MD 10 (Figure 4 (c, d)) favors CMD. As a further verification, the Spearman correlation between CMD and MD 121 is 0.980 (H_0) and 0.993 (H_1), compared to 0.926 (H_0) and 0.955 (H_1) for MD 10 vs MD 121. This confirms that CMD agrees more with the fine-grid MD than its coarser version, while maintaining a computational cost comparable to the latter.

7.2 Classification of synthetic shapes

As a second experiment, we use CMD, MD 121, and MD 10 directly as classifiers in a k -nearest neighbors framework. For each test sample, we compute the $k = 3$ nearest neighbors in both H_0 and H_1 separately. We then select the prediction from the homological dimension with higher confidence, defined as the proportion of the k neighbors voting for the most common class. In case of equal confidence, we use the average distance as a tiebreaker. We generate five classes of 3D point clouds in $[0, 1]^3$: circle, sphere, torus, three clusters, and two concentric circles. We refer to Figure 5 for examples of point clouds

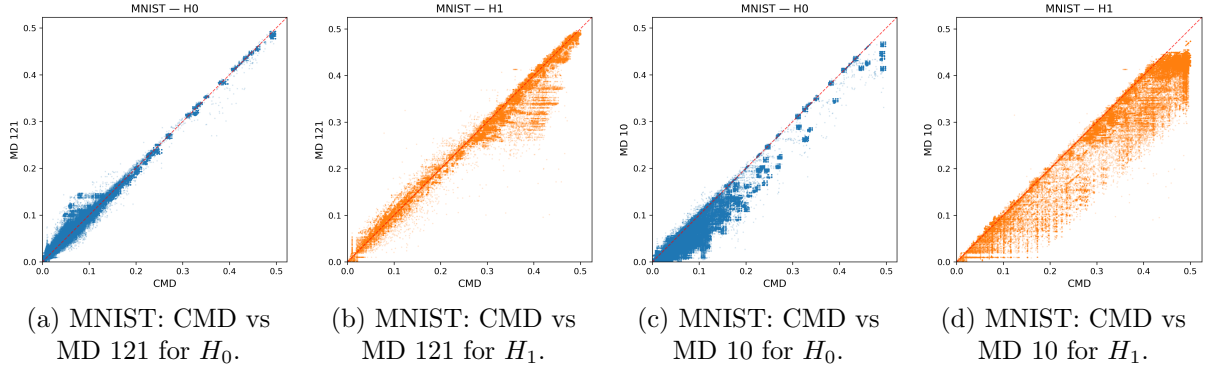


Figure 4: Distance comparison for MNIST. (a,b) CMD vs MD 121 for H_0 and H_1 . (c,d) CMD vs MD 10 for H_0 and H_1 . Red dashed line shows $y = x$.

for each class, colored by eccentricity. The bifiltration uses φ_1 as the distance to the 15-th neighbor (codensity), and φ_2 as eccentricity [43], both normalized to $[0, 1]$. Persistence is computed via Alpha complex with lower-star extension. Each class contains 40 samples, and we test across additive Gaussian noise levels $\sigma \in \{0.00, 0.03, 0.06, 0.09, 0.12\}$ applied independently to each coordinate of the point cloud, and number of points in the point cloud $n \in \{500, 1000, 5000\}$. As single-parameter baselines, we compute both codensity lower-star and eccentricity lower-star persistence. Table 1 reports classification accuracies (mean \pm standard deviation) across all combinations of sample size n and noise level σ . The results are consistent across all configurations: CMD and MD 121 achieve comparable performance throughout, while MD 10 systematically underperforms. The key difference emerges at high sample size and moderate-to-high noise. At $n = 5000$, $\sigma = 0.06$: CMD achieves 97.5%, surpassing MD 121 (94.2%), while MD 10 drops to 80.8%. At $\sigma = 0.12$: CMD (78.2%) and MD 121 (81.0%) remain comparable, while MD 10 falls to 58.0%. Figure 6 visualizes this trend for $n = 5000$, showing that CMD maintains robust performance as noise increases, while MD 10 degrades significantly at $\sigma \geq 0.09$. Notably, MD 10 performs comparably to the best single-parameter baseline (codensity lower-star, see Table 2), while CMD and MD 121 substantially outperform all 1-PH methods, confirming that the second filtration carries complementary discriminative information.

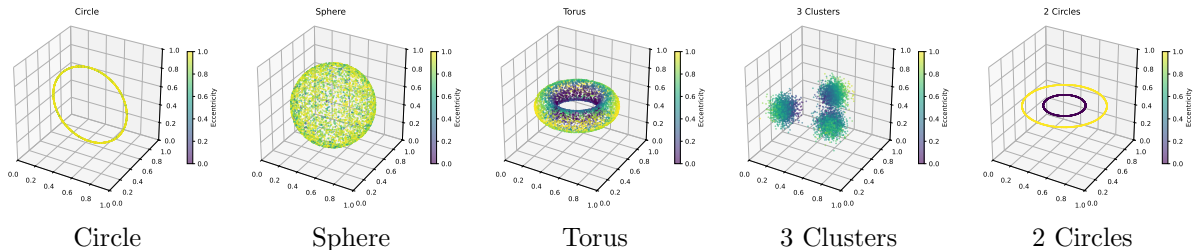


Figure 5: Examples of synthetic 3D point clouds for each class ($n = 5000$, $\sigma = 0.0$), colored by eccentricity.

Table 1: Classification accuracy (%) on synthetic shapes.

σ	$n = 500$			$n = 1000$			$n = 5000$		
	CMD	MD 121	MD 10	CMD	MD 121	MD 10	CMD	MD 121	MD 10
0.00	91.8 \pm 5.3	91.0 \pm 6.2	91.3 \pm 5.6	94.5 \pm 3.9	92.5 \pm 6.4	93.3 \pm 4.1	99.3 \pm 0.8	99.8 \pm 0.5	99.0 \pm 1.1
0.03	85.2 \pm 2.8	88.0 \pm 4.0	84.5 \pm 3.4	94.5 \pm 2.5	94.2 \pm 1.5	93.3 \pm 2.7	99.3 \pm 0.8	98.5 \pm 0.9	97.2 \pm 2.2
0.06	76.0 \pm 3.3	80.7 \pm 4.4	69.5 \pm 5.1	89.0 \pm 2.4	92.5 \pm 3.6	78.0 \pm 7.4	97.5 \pm 1.9	94.2 \pm 2.5	80.8 \pm 4.2
0.09	74.0 \pm 5.9	75.0 \pm 5.3	70.3 \pm 1.9	77.3 \pm 6.4	82.3 \pm 6.3	78.8 \pm 6.9	88.5 \pm 2.8	89.0 \pm 3.2	86.3 \pm 2.6
0.12	69.0 \pm 4.8	69.3 \pm 4.9	64.0 \pm 5.7	69.5 \pm 5.2	74.0 \pm 5.4	70.0 \pm 5.8	78.2 \pm 2.8	81.0 \pm 3.5	58.0 \pm 5.2

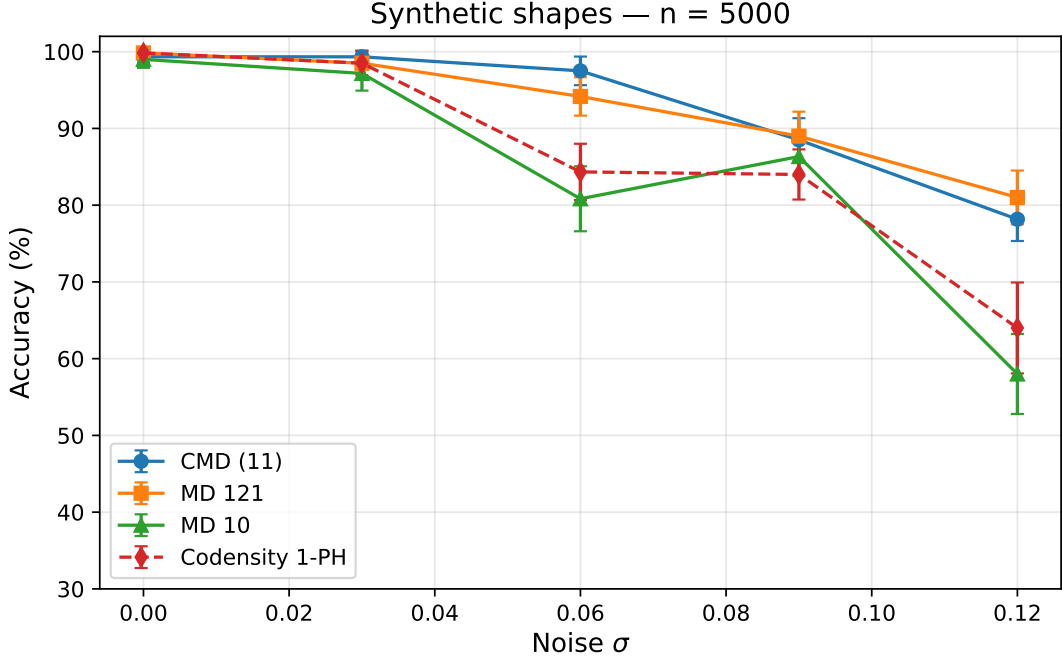


Figure 6: Classification accuracy vs noise for synthetic shapes at $n = 5000$. CMD maintains robust performance across all noise levels, while MD 10 degrades significantly at high noise ($\sigma \geq 0.09$).

Table 2: Single-parameter baseline accuracies (%) on synthetic shapes.

σ	$n = 500$		$n = 1000$		$n = 5000$	
	Codensity LS	Ecc LS	Codensity LS	Ecc LS	Codensity LS	Ecc LS
0.00	83.7 ± 3.7	75.2 ± 5.6	93.2 ± 3.4	71.3 ± 7.8	99.8 ± 0.5	78.3 ± 6.1
0.03	75.0 ± 6.2	24.2 ± 3.7	91.8 ± 4.4	23.5 ± 4.2	98.5 ± 1.6	25.0 ± 4.0
0.06	77.0 ± 4.0	20.5 ± 2.5	81.7 ± 3.9	22.0 ± 2.9	84.3 ± 3.7	21.0 ± 4.9
0.09	76.7 ± 5.8	19.2 ± 3.0	78.0 ± 4.6	24.8 ± 6.8	84.0 ± 3.3	28.3 ± 8.9
0.12	62.5 ± 4.8	21.3 ± 2.2	69.3 ± 3.5	22.2 ± 6.4	64.0 ± 5.9	25.3 ± 5.2

7.3 Classification of chaotic attractors

Lastly, we classify five chaotic dynamical systems: Lorenz, Rössler, Thomas, Sprott, and Four-Wing attractors. Chaotic attractors have been widely studied in the topological data analysis literature [34, 36, 44, 46]. Each trajectory is sampled with $n = 500$ points and rescaled to $[0, 1]^3$. The bifiltration uses $\varphi_1 = \sqrt{\alpha}$ (Alpha complex filtration values, clipped at 0.15 for numerical stability) and $\varphi_2 = \text{eccentricity}$ (lower-star extension). Clipping avoids degenerate filtration values arising from quasi-coplanar points. We generate 40 samples per class. We refer to Figure 7 for visual examples of trajectories from each attractor class. The considered approximation of the convex matching distance performs comparably in this dataset to the two approximations of the matching distance: CMD $95.2 \pm 1.9\%$, MD 121 $96.5 \pm 2.4\%$, and MD 10 $93.8 \pm 3.4\%$. In fact, the topological signal is strong enough that even a coarse approximation of the matching distance suffices. However, a distance quality analysis as in Section 7.1 (Figure 8) reveals that CMD and MD 121 agree more closely with each other than either does with MD 10, consistent with our previous findings.

7.4 Computational cost

We evaluate execution time on a subset of MNIST (150 images). The cost of computing the distance is dominated by persistence diagram computations and bottleneck distance evaluations. Table 3 reports timings for the three approximation strategies.

The observed speedups of MD 121 and MD 10 over CMD is lower than the theoretical ratio due to

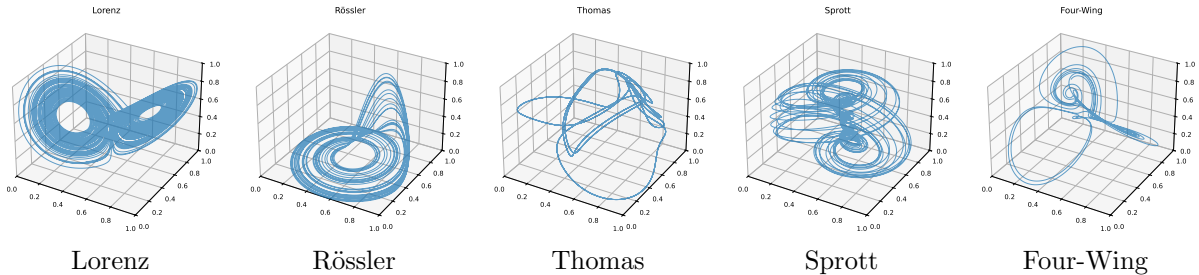
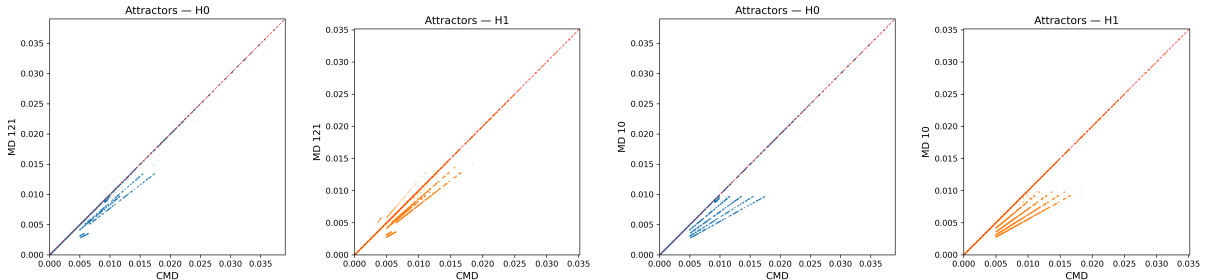


Figure 7: Examples of attractors trajectories.



(a) Attractors: CMD vs MD 121 for H_0 . (b) Attractors: CMD vs MD 121 for H_1 . (c) Attractors: CMD vs MD 10 for H_0 . (d) Attractors: CMD vs MD 10 for H_1 .

Figure 8: Distance comparison for the attractors dataset. (a,b) CMD vs MD 121 for H_0 and H_1 . (c,d) CMD vs MD 10 for H_0 and H_1 . Red dashed line shows $y = x$.

differences in persistence diagram sizes. The matching distance parametrisation produces on average smaller and sparser diagrams, especially for a, b close to 0 and 1. This reduces the cost per bottleneck distance computation. Nevertheless, CMD achieves nearly identical execution time to MD 10 while providing substantially better approximation quality.

8 Conclusions

In this work, we introduced the convex matching distance, a new pseudo-metric to compare functions with values in \mathbb{R}^2 . If φ and ψ are two such functions, the convex matching distance is defined by maximising the bottleneck distance between the persistence diagrams of the convex combinations φ^t and ψ^t of the coordinates of φ and ψ . Whereas the classical matching distance requires the computation of a two-parameter family of persistence diagrams (see [20, 4, 32]), our metric depends only on the one-parameter family indexed by $t \in [0, 1]$. This reduction in dimensionality, combined with the additional regularity of the operator sending φ to φ^t , leads to both conceptual simplifications and computational advantages improving the effective computability of the metric. Moreover, the smoothness preservation property of the proposed operator allows for its incorporation into learning-based frameworks, ensuring stable and well-behaved gradients and enabling the use of standard optimization and training procedures.

Under generic regularity assumptions on the input functions, we show in Theorem 3 that the convex matching distance is realised at some parameter in a distinguished subset of $[0, 1]$, that we called special set. We conjecture that this subset is finite under generic conditions on the input pair (φ, ψ) . It is not hard to find examples of pairs of functions having an infinite special set. For example, this happens when $\text{Ctr}(\varphi, \psi)$ contains two contours such that one is the translated of the other, or when a contour has zero curvature. However, in our opinion, these phenomena occur when the pair of functions is not generic, as the functions can be infinitesimally modified locally, so not to have this properties any more.

We validated the practical effectiveness of the convex matching distance through experiments on MNIST, synthetic 3D shapes under varying noise levels, and chaotic dynamical attractors. Our results demonstrate that the convex matching distance achieves accuracy comparable to the full matching distance computed on a fine 11×11 parameter grid, while requiring approximately $10\times$ fewer persistence diagram computations. Moreover, the convex matching distance substantially outperforms coarser approximations of the matching distance, confirming that the convex parametrization effectively captures the discriminative information of the bifiltration.

Table 3: Wall-clock time (seconds) for distance matrix computation on MNIST subset (150 images).

Method	PD computations	Bottleneck distances	Total
CMD	1.3s	1.5s	2.8s (1.0×)
MD 121	13.2s	12.2s	25.4s (9.0×)
MD 10	1.2s	1.1s	2.2s (0.8×)

Future work will focus on the effective computation of the parameters belonging to this special set as well as on the identification of the proper genericity assumptions under which such a set is finite. Moreover, we aim to weaken the assumptions under which we proved Theorem 3 and to prove their genericity.

Finally, as mentioned in the introduction the operator that given a parameter t maps each function φ to the function φ^t is just one of the infinitely many possibilities for assigning a parametric family of functions to φ . In the near future, we intend to investigate alternative operators and evaluate the advantages and drawbacks associated with their adoption.

Acknowledgements

F.C. was funded by Inria. P.F. was supported by GNSAGA-INdAM, CNIT National Laboratory WiLab, and the WiLab-Huawei Joint Innovation Center. U.F. acknowledges the Italian National Biodiversity Future Center (NBFC) - National Recovery and Resilience Plan (NRRP) funded by the EU-NextGenerationEU (project code CN 00000033) and the Innovation Ecosystem Robotics and AI for Socio-economic Empowerment (RAISE) - National Recovery and Resilience Plan (NRRP) funded by the EU-NextGenerationEU (project code ECS 00000035). E.M.G. was supported by GNAMPA-INdAM and GNAMPA Project CUP E53C22001930001. N.Q. was supported by CNIT National Laboratory WiLab, and the WiLab-Huawei Joint Innovation Center. S.S. acknowledges the GNSAGA-INdAM and the MUR Excellence Department Project MatMod@TOV awarded to the Department of Mathematics, University of Rome Tor Vergata, CUP E83C23000330006. F.T. was funded by the Knut and Alice Wallenberg Foundations and the WASP Postdoctoral Scholarship Program.

References

- [1] Faraz Ahmad. Compactification of perception pairs and spaces of group equivariant non-expansive operators. *Topology and its Applications*, 378:109668, 2026. URL: <https://www.sciencedirect.com/science/article/pii/S0166864125004663>, doi:10.1016/j.topol.2025.109668.
- [2] Faraz Ahmad, Massimo Ferri, and Patrizio Frosini. Generalized permutants and graph GENEOS. *Machine Learning and Knowledge Extraction*, 5(4):1905–1920, 2023. URL: <https://www.mdpi.com/2504-4990/5/4/92>.
- [3] Madjid Allili, Tomasz Kaczynski, and Claudia Landi. Reducing complexes in multidimensional persistent homology theory. *J. Symbolic Comput.*, 78:61–75, 2017. doi:10.1016/j.jsc.2015.11.020.
- [4] Asilata Bapat, Robyn Brooks, Celia Hacker, Claudia Landi, Barbara I. Mahler, and Elizabeth R. Stephenson. Computing the matching distance of 2-parameter persistence modules from critical values. *arXiv e-prints*, October 2022. doi:10.48550/arXiv.2210.12868.
- [5] Mattia G. Bergomi, Patrizio Frosini, Daniela Giorgi, and Nicola Quercioli. Towards a topological–geometrical theory of group equivariant non-expansive operators for data analysis and machine learning. *Nature Machine Intelligence*, 1(9):423–433, 2019.
- [6] Nicolas Berkouk and François Petit. Projected distances for multi-parameter persistence modules. *Annales de l’Institut Fourier*, Online first:62, 2026.
- [7] S. Biasotti, A. Cerri, P. Frosini, D. Giorgi, and C. Landi. Multidimensional size functions for shape comparison. *J. Math. Imaging Vision*, 32(2):161–179, 2008. doi:10.1007/s10851-008-0096-z.

- [8] Silvia Biasotti, Andrea Cerri, Patrizio Frosini, and Daniela Giorgi. A new algorithm for computing the 2-dimensional matching distance between size functions. *Pattern Recognition Letters*, 32(14):1735–1746, 2011. doi:10.1016/j.patrec.2011.07.014.
- [9] Håvard Bakke Bjerkevik and Michael Kerber. Asymptotic improvements on the exact matching distance for 2-parameter persistence. *J. Comput. Geom.*, 14(1):309–342, 2023. doi:10.3982/qe2088.
- [10] Giovanni Bocchi, Stefano Botteghi, Martina Brasini, Patrizio Frosini, and Nicola Quercioli. On the finite representation of linear group equivariant operators via permutant measures. *Annals of Mathematics and Artificial Intelligence*, 91:1–23, 02 2023. doi:10.1007/s10472-022-09830-1.
- [11] Giovanni Bocchi, Massimo Ferri, and Patrizio Frosini. A novel approach to graph distinction through GENEOS and permutants. *Scientific Reports*, 15(1):6259, Feb 2025. doi:10.1038/s41598-025-90152-7.
- [12] Giovanni Bocchi, Patrizio Frosini, Alessandra Micheletti, Alessandro Pedretti, Gianluca Palermo, Davide Gadioli, Carmen Gratteri, Filippo Lunghini, Andrea Rosario Beccari, Anna Fava, and Carmine Talarico. A geometric XAI approach to protein pocket detection. In Luca Longo, Weiru Liu, and Grégoire Montavon, editors, *Joint Proceedings of the xAI 2024 Late-breaking Work, Demos and Doctoral Consortium co-located with the 2nd World Conference on eXplainable Artificial Intelligence (xAI-2024), Valletta, Malta, July 17-19, 2024*, volume 3793 of *CEUR Workshop Proceedings*, pages 217–224. CEUR-WS.org, 2024. URL: https://ceur-ws.org/Vol-3793/paper_28.pdf.
- [13] Giovanni Bocchi, Patrizio Frosini, Alessandra Micheletti, Alessandro Pedretti, Gianluca Palermo, Davide Gadioli, Carmen Gratteri, Filippo Lunghini, Akash Deep Biswas, Pieter F. W. Stouten, Andrea R. Beccari, Anna Fava, and Carmine Talarico. GENEOnet: a breakthrough in protein binding pocket detection using group equivariant non-expansive operators. *Scientific Reports*, 15(1):34597, Oct 2025. doi:10.1038/s41598-025-18132-5.
- [14] Francesca Cagliari, Barbara Di Fabio, and Massimo Ferri. One-dimensional reduction of multidimensional persistent homology. *Proc. Amer. Math. Soc.*, 138(8):3003–3017, 2010. doi:10.1090/S0002-9939-10-10312-8.
- [15] Francesca Cagliari and Claudia Landi. Finiteness of rank invariants of multidimensional persistent homology groups. *Appl. Math. Lett.*, 24(4):516–518, 2011. doi:10.1016/j.aml.2010.11.004.
- [16] Gunnar Carlsson, Gurjeet Singh, and Afra Zomorodian. Computing multidimensional persistence. *J. Comput. Geom.*, 1(1):72–100, 2010. doi:10.20382/jocg.v1i1a6.
- [17] Gunnar Carlsson and Afra Zomorodian. The theory of multidimensional persistence. *Discrete Comput. Geom.*, 42(1):71–93, 2009. doi:10.1007/s00454-009-9176-0.
- [18] N. Cavazza, M. Ethier, P. Frosini, T. Kaczynski, and C. Landi. Comparison of persistent homologies for vector functions: from continuous to discrete and back. *Comput. Math. Appl.*, 66(4):560–573, 2013. doi:10.1016/j.camwa.2013.06.004.
- [19] Niccolò Cavazza, Massimo Ferri, and Claudia Landi. Estimating multidimensional persistent homology through a finite sampling. *International Journal of Computational Geometry & Applications*, 25(03):187–205, 2015. doi:10.1142/S0218195915500119.
- [20] Andrea Cerri, Barbara Di Fabio, Massimo Ferri, Patrizio Frosini, and Claudia Landi. Betti numbers in multidimensional persistent homology are stable functions. *Mathematical Methods in the Applied Sciences*, 36(12):1543–1557, 2013. doi:10.1002/mma.2704.
- [21] Andrea Cerri, Marc Ethier, and Patrizio Frosini. On the geometrical properties of the coherent matching distance in 2D persistent homology. *J. Appl. Comput. Topol.*, 3(4):381–422, 2019. doi:10.1007/s41468-019-00041-y.
- [22] Andrea Cerri and Patrizio Frosini. Necessary conditions for discontinuities of multidimensional persistent Betti numbers. *Mathematical Methods in the Applied Sciences*, 38(4):617–629, 2015. doi:10.1002/mma.3093.

- [23] Andrea Cerri and Claudia Landi. The persistence space in multidimensional persistent homology. In Rocio Gonzalez-Diaz, Maria-Jose Jimenez, and Belen Medrano, editors, *Discrete Geometry for Computer Imagery*, pages 180–191, Berlin, Heidelberg, 2013. Springer Berlin Heidelberg.
- [24] David Cohen-Steiner, Herbert Edelsbrunner, and John Harer. Stability of persistence diagrams. *Discrete & Computational Geometry*, 37(1):103–120, Jan 2007. doi:10.1007/s00454-006-1276-5.
- [25] Jacopo Joy Colombini, Filippo Bonchi, Francesco Giannini, Fosca Giannotti, Roberto Pellungrini, and Patrizio Frosini. Mathematical foundation of interpretable equivariant surrogate models. In Riccardo Guidotti, Ute Schmid, and Luca Longo, editors, *Explainable Artificial Intelligence*, pages 294–318, Cham, 2026. Springer Nature Switzerland.
- [26] Michele d’Amico, Patrizio Frosini, and Claudia Landi. Natural pseudo-distance and optimal matching between reduced size functions. *Acta Applicandae Mathematicae*, 109(2):527–554, Feb 2010. doi:10.1007/s10440-008-9332-1.
- [27] Marc Ethier, Patrizio Frosini, Nicola Quercioli, and Francesca Tombari. Geometry of the matching distance for 2D filtering functions. *Journal of Applied and Computational Topology*, 7(4):815–830, Dec 2023. doi:10.1007/s41468-023-00128-7.
- [28] Raúl Felipe. GENEOS with respect to the projective Hilbert metric. *The Journal of Geometric Analysis*, 35(9):264, Jul 2025. doi:10.1007/s12220-025-02102-4.
- [29] P. Frosini. Towards an observer-oriented theory of shape comparison: position paper. In *Proceedings of the Eurographics 2016 Workshop on 3D Object Retrieval*, 3DOR ’16, page 5–8, Goslar, DEU, 2016. Eurographics Association.
- [30] Patrizio Frosini. Connections between size functions and critical points. *Mathematical Methods in the Applied Sciences*, 19(7):555–569, 1996. doi:10.1002/(SICI)1099-1476(19960510)19:7<555::AID-MMA787>3.0.CO;2-X.
- [31] Patrizio Frosini and Grzegorz Jabłoński. Combining persistent homology and invariance groups for shape comparison. *Discrete & Computational Geometry*, 55(2):373–409, Mar 2016. doi:10.1007/s00454-016-9761-y.
- [32] Patrizio Frosini, Eloy Mósig García, Nicola Quercioli, and Francesca Tombari. Matching distance via the extended Pareto grid. *SIAM J. Appl. Algebra Geom.*, 9(3):554–576, 2025. doi:10.1137/24M1680398.
- [33] Patrizio Frosini and Michele Mulazzani. Size homotopy groups for computation of natural size distances. *Bull. Belg. Math. Soc. Simon Stevin*, 6(3):455–464, 1999.
- [34] T. Gowdrige, N. Dervilis, and K. Worden. On topological data analysis for structural dynamics: An introduction to persistent homology. *ASME Open Journal of Engineering*, 1:011038, 09 2022. arXiv:https://asmedigitalcollection.asme.org/openengineering/article-pdf/doi/10.1115/1.4055184/6914412/aoje_1_011038.pdf, doi:10.1115/1.4055184.
- [35] Heather A. Harrington, Nina Otter, Hal Schenck, and Ulrike Tillmann. Stratifying multiparameter persistent homology. *SIAM J. Appl. Algebra Geom.*, 3(3):439–471, 2019. doi:10.1137/18M1224350.
- [36] W Hussain Shah, S Rafia Fatima, G Huerta-Cuellar, JH García-López, CG Mata Ramirez, and R Jaimes-Reátegui. Topological data analysis approach to time series and shape analysis of dynamical system. *Chaos: An Interdisciplinary Journal of Nonlinear Science*, 35(6), 2025.
- [37] Michael Kerber, Michael Lesnick, and Steve Oudot. Exact computation of the matching distance on 2-parameter persistence modules. *J. Comput. Geom.*, 11(2):4–25, 2020. doi:10.20382/jocg.v11i2a2.
- [38] Diogo Lavado, Alessandra Micheletti, Giovanni Bocchi, Patrizio Frosini, and Cláudia Soares. SCENE-Net: Geometric induction for interpretable and low-resource 3D pole detection with Group-Equivariant Non-Expansive Operators. *Computer Vision and Image Understanding*, 262:104531, 2025. URL: https://www.sciencedirect.com/science/article/pii/S1077314225002541, doi:10.1016/j.cviu.2025.104531.

- [39] Michael Lesnick. The theory of the interleaving distance on multidimensional persistence modules. *Found. Comput. Math.*, 15(3):613–650, 2015. doi:10.1007/s10208-015-9255-y.
- [40] Clément Maria, Jean-Daniel Boissonnat, Marc Glisse, and Mariette Yvinec. The gudhi library: Simplicial complexes and persistent homology. In Hoon Hong and Chee Yap, editors, *Mathematical Software – ICMS 2014*, pages 167–174, Berlin, Heidelberg, 2014. Springer Berlin Heidelberg.
- [41] Alessandra Micheletti. A new paradigm for artificial intelligence based on group equivariant non-expansive operators. *European Mathematical Society Magazine*, 128:4–12, 2023. doi:10.4171/MAG/133.
- [42] D. J. Simms. J. Milnor, Morse Theory, Annals of Mathematics Studies 51 (Princeton University Press, 1963), vi + 153 pp., 24s. *Proceedings of the Edinburgh Mathematical Society*, 14(1):84–84, 1964. doi:10.1017/S0013091500011330.
- [43] Gurjeet Singh, Facundo Mémoli, and Gunnar Carlsson. Topological methods for the analysis of high dimensional data sets and 3d object recognition. 4th Symposium on Point Based Graphics, PBG@Eurographics 2007, pages 91–100, 2007.
- [44] Joshua R. Tempelman and Firas A. Khasawneh. A look into chaos detection through topological data analysis. *Physica D: Nonlinear Phenomena*, 406:132446, 2020. URL: <https://www.sciencedirect.com/science/article/pii/S0167278919300739>, doi:10.1016/j.physd.2020.132446.
- [45] Katharine Turner, Sayan Mukherjee, and Doug M. Boyer. Persistent homology transform for modeling shapes and surfaces. *Information and Inference: A Journal of the IMA*, 3(4):310–344, 2014. doi:10.1093/imaia/iaiu011.
- [46] Vinay Venkataraman, Karthikeyan Natesan Ramamurthy, and Pavan Turaga. Persistent homology of attractors for action recognition. In *2016 IEEE International Conference on Image Processing (ICIP)*, pages 4150–4154, 2016. doi:10.1109/ICIP.2016.7533141.
- [47] Y. H. Wan. Morse theory for two functions. *Topology*, 14(3):217–228, 1975. doi:10.1016/0040-9383(75)90002-6.